The Astrophysical Journal Letters, 771:L44 (7pp), 2013 July 10 doi:10.1088/2041-8205/771/2/L44

DISCOVERY OF A 7 mHz X-RAY QUASI-PERIODIC OSCILLATION FROM THE MOST MASSIVE STELLAR-MASS BLACK HOLE IC 10 X-1

Dheeraj R. Pasham[1], Tod E. Strohmayer[2], and Richard F. Mushotzky[1]
[1] Astronomy Department, University of Maryland, College Park, MD 20742, USA; dheeraj@astro.umd.edu, richard@astro.umd.edu
[2] Astrophysics Science Division, NASA's Goddard Space Flight Center, Greenbelt, MD 20771, USA; tod.strohmayer@nasa.gov
Received 2013 May 31; accepted 2013 June 14; published 2013 June 27

ABSTRACT

We report the discovery with *XMM-Newton* of an ≈7 mHz X-ray (0.3–10.0 keV) quasi-periodic oscillation (QPO) from the eclipsing, high-inclination black hole binary IC 10 X-1. The QPO is significant at $>4.33\sigma$ confidence level and has a fractional amplitude (% rms) and a quality factor, $Q \equiv \nu/\Delta\nu$, of ≈11 and 4, respectively. The overall X-ray (0.3–10.0 keV) power spectrum in the frequency range 0.0001–0.1 Hz can be described by a power-law with an index of ≈−2, and a QPO at 7 mHz. At frequencies $\gtrsim$0.02 Hz there is no evidence for significant variability. The fractional amplitude (rms) of the QPO is roughly energy-independent in the energy range of 0.3–1.5 keV. Above 1.5 keV the low signal-to-noise ratio of the data does not allow us to detect the QPO. By directly comparing these properties with the wide range of QPOs currently known from accreting black hole and neutron stars, we suggest that the 7 mHz QPO of IC 10 X-1 may be linked to one of the following three categories of QPOs: (1) the "heartbeat" mHz QPOs of the black hole sources GRS 1915+105 and IGR J17091−3624, or (2) the 0.6–2.4 Hz "dipper QPOs" of high-inclination neutron star systems, or (3) the mHz QPOs of Cygnus X-3.

Key words: black hole physics – X-rays: binaries – X-rays: individual (IC 10 X-1)

1. INTRODUCTION

The X-ray light curves of numerous accreting neutron star and stellar-mass black holes (StMBHs) show evidence for the presence of quasi-periodic oscillations (QPOs), which appear as finite-width peaks in their power density spectra (PDS; see van der Klis 2006 and McClintock & Remillard 2006 for reviews of neutron star and StMBH QPOs). While it is known that QPOs occur with a wide range of centroid frequencies—a few mHz to above a kHz in neutron stars and a few mHz to a few hundred Hz in the case of StMBHs—the exact nature of the physical processes producing such oscillations is still a mystery.

Based on the observed properties, that is, their centroid frequencies, widths, amplitudes, and overall nature of their power spectra, etc., QPOs have been categorized into different groups. In neutron star binaries the QPO phenomenon constitutes the *kilohertz* QPOs (centroid frequencies in the range of 300–1200 Hz; see the review by van der Klis 2000) seen from over two dozen sources (e.g., Méndez et al. 2001; Barret et al. 2008 and references therein), the *hectohertz* QPOs (∼100–300 Hz; e.g., van Straaten et al. 2003; Altamirano et al. 2008a) seen predominantly in a special class (atoll) of neutron star binaries, the low-frequency QPOs (0.01–50 Hz; e.g., van Straaten et al. 2003), the 1 Hz QPOs observed in two accreting millisecond X-ray pulsars (AMXPs; e.g., Wijnands 2004), the ≈0.6–2.4 Hz QPOs observed only from dipping (high-inclination) neutron star binaries (e.g., Homan et al. 1999; Jonker et al. 1999, 2000) and the very low-frequency 7–15 mHz QPOs observed from at least three systems (e.g., Revnivtsev et al. 2001; Altamirano et al. 2008b).

Similarly, black holes also show a variety of QPOs (McClintock & Remillard 2006). They can be broadly classified into two categories: (1) high-frequency QPOs (HFQPOs) with centroid frequencies in the range of a few×(10–100) Hz (e.g., Miller et al. 2001; Strohmayer 2001; Remillard et al. 2006; Belloni & Altamirano 2013) and (2) low-frequency QPOs (LFQPOs) that occur in the range of 0.1–15 Hz (e.g., Casella et al. 2005). Based on their broadband properties, viz., shape, fractional amplitude of the PDS and the QPOs, etc., the LFQPOs have been further sub-divided into type-A, B, and C (e.g., Homan et al. 2001; Remillard et al. 2002). In addition to the HFQPOs and the LFQPOs of StMBHs, two black hole sources, GRS 1915+105 and IGR J17091−3624, show so-called "heartbeat" QPOs which occur in the mHz frequency regime (e.g., Belloni et al. 2000; Altamirano et al. 2011). Furthermore, some ultraluminous X-ray sources (ULXs) show a few×10 mHz QPOs (e.g., Dewangan et al. 2006; Pasham & Strohmayer 2013). More recently, an 11 mHz X-ray QPO and the recurrence of a few×mHz QPOs were detected from the black hole candidates H1743−322 and Cygnus X-3, respectively (Koljonen et al. 2011; Altamirano & Strohmayer 2012).

IC 10 X-1 is an eclipsing, Wolf–Rayet binary containing the most massive StMBH known with an estimated black hole mass of 23–34 $M_{\odot}$ (Prestwich et al. 2007; Silverman & Filippenko 2008). The presence of an eclipse suggests that the system is highly inclined, i.e., close to edge-on. This source was observed previously with *XMM-Newton* (ID: 0152260101) for a duration of roughly 45 ks. After accounting for background flaring only a mere 15 ks of useful data was available, analysis of which showed some evidence—although at modest statistical significance—for the presence of a QPO at ≈7 mHz. Motivated by this, and to carry out eclipse mapping, a long *XMM-Newton* observation was proposed to confirm the presence of this mHz QPO (ID: 0693390101; PI: Strohmayer). Here we present results from our timing analysis of this new data set and confirm the presence of the QPO at 7 mHz.

2. *XMM-NEWTON* OBSERVATIONS

Beginning 2012 August 18 at 22:05:46 (UTC) *XMM-Newton* observed IC 10 X-1 for roughly 135 ks, a duration approximately equal to its orbital period (34.93 hr; Prestwich et al. 2007; Silverman & Filippenko 2008). For our study, we only used the EPIC data (both pn and MOS). We used the latest standard analysis system version 13.0.0 for extracting the images and the event lists. The source was easily identifiable and there were no source confusion problems (see Figure 1). The source events

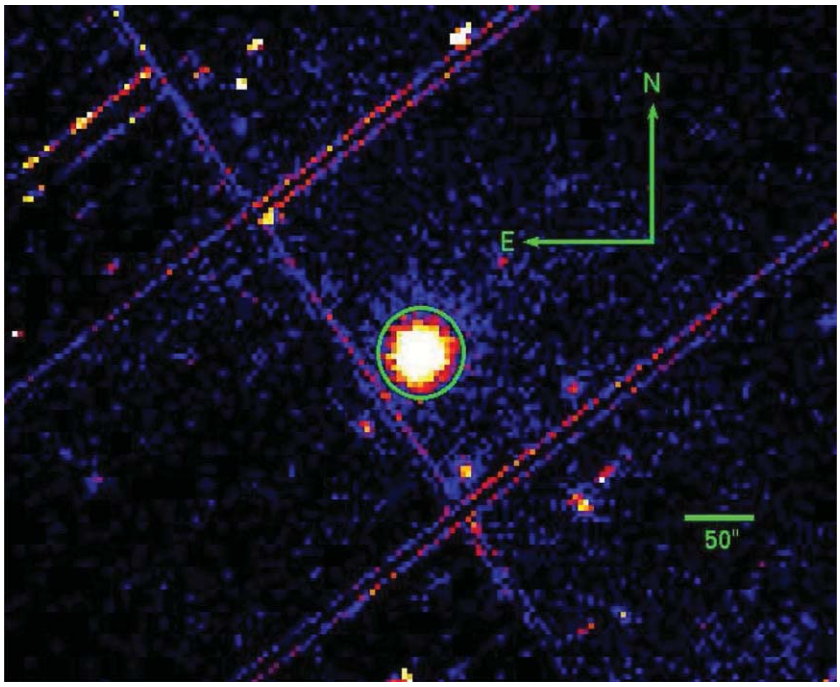

Figure 1. EPIC-pn X-ray (0.3–10.0 keV) image of IC 10 X-1. Clearly there is only one point source, IC 10 X-1, and no obvious evidence for source contamination. The extraction region of radius 33″ is indicated by a green circle.

were extracted from a circular region of radius 33″ centered around the source and the background events were extracted from a nearby circular region of the same size. The observation was affected by flaring only briefly at the very beginning and the end of the pointing. These epochs were removed from our analysis.

The combined pn and MOS 0.3–10.0 keV light curve of IC 10 X-1 is shown in Figure 2 (black) along with the background (red). Also overlaid are the good time intervals (GTIs) during which a given EPIC instrument (pn/MOS1/MOS2) was continuously active for more than 5 ks. For a given instrument the horizontal line, which is offset to an arbitrary value, indicates the active time, while a vertical line marks the beginning or the end of a continuous GTI. It is clear that EPIC-pn has three GTIs of duration roughly 23 ks, 75 ks and 27 ks, while MOS1 has two GTIs of length 30 ks and 99 ks and MOS2 has one long GTI of 130 ks.

3. RESULTS

It is clear even by eye that the source varies significantly. Since the pn detector offers the highest effective area among the three EPIC instruments, we started our analysis with its longest available GTI of $\approx$75 ks (between hour 8.5 and 29.5 in Figure 2). Using all the 0.3–10.0 keV photons we constructed a Leahy-normalized PDS where the Poisson noise equals 2 (Leahy et al. 1983). This is shown in the top left panel of Figure 3 (histogram). It is evident that the overall power spectrum can be described by a simple power-law noise at the lowest frequencies with a QPO-like feature around 7 mHz and essentially Poisson noise at frequencies above $\gtrsim$0.02 Hz. In order to test the significance of the QPO we followed a rigorous Monte Carlo approach described below.

First, we fit the continuum of the PDS using a model consisting of a power-law plus a constant. While modeling the continuum we used the frequency range 0.0001 (the lowest that can be probed)–0.1 Hz and excluded the region containing the apparent QPO feature, i.e., 5–9 mHz. The best-fit continuum model parameters are shown in the first column of Table 1. Thereafter, following the prescription described by Timmer & Koenig (1995), we simulated a large number of light curves (and their corresponding PDS) that have the same shape, i.e., same parameters, as in the first column of Table 1, and the same frequency resolution as the spectrum used for obtaining the best-fit continuum parameters. A sample PDS simulated with the above technique (red) along with the real PDS (black) is shown in the top right panel of Figure 3. We simulated 370 such power spectra and found the maximum value in each frequency bin. This gave us the 99.73% (3σ) significance within that particular bin. A similar estimate for each frequency bin gave us the complete confidence curve. Similarly we simulated 10,000 PDS and estimated the 99.99% (3.9σ) confidence curve. It should be noted that the confidence curves are sensitive to the chosen values of the continuum model parameters. Given the error on each of the individual model parameters, i.e., best-fit power-law normalization and the power-law index, we estimated the 99.73% and the 99.99% curves for various combinations of the power-law normalization and the index within the error bars quoted in Column 1 of Table 1. To be conservative we picked the maximum of these curves. These confidence levels are overlaid in the figure. It is clear that the QPO feature is significant at the 99.99% level.

To further confirm the presence of this QPO feature, we extracted another PDS using the combined MOS data. For this purpose we used the longer GTI of roughly 95 ks (from hour 8.5 to hour 34.5 in Figure 2). The 0.3–10.0 keV combined MOS PDS is shown in the bottom left panel of Figure 3. The QPO feature is again evident at 7 mHz. To quantify the variability we first modeled the PDS with a power-law plus a constant. This gave a χ^2 of 245 with 192 degrees of freedom (dofs). We then added a Lorentzian component to model the QPO feature at 7 mHz. This improved the χ^2 by 28 with an addition of three

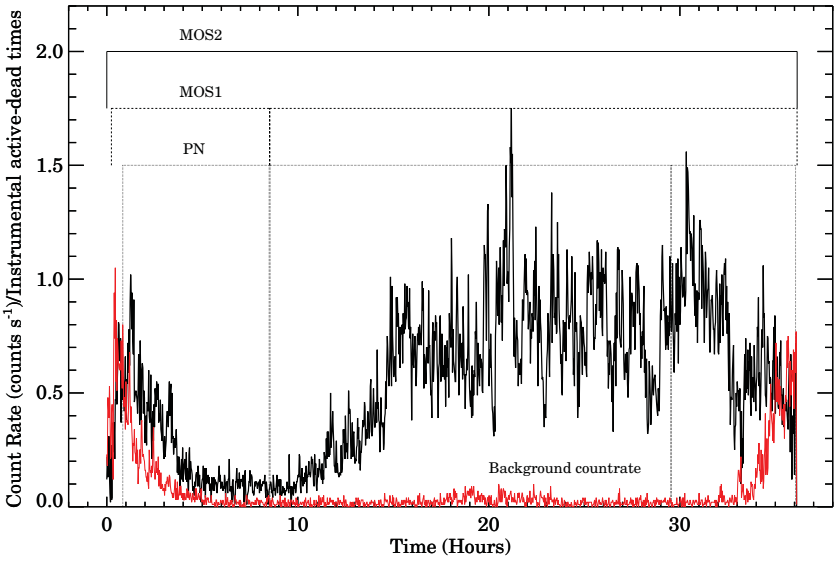

Figure 2. The combined, background-subtracted EPIC X-ray (0.3–10.0 keV) light curve of IC 10 X-1 (black) along with the background light curve (red). Time zero corresponds to 4.6171485×10^8 s since 50814.0 (Modified Julian Date). Both the light curves were binned to 100 s. The start and end times of all the GTIs greater than 5 ks are indicated by vertical lines (see text).

Table 1
Summary of Power Spectral Modeling

Parameter	EPIC-pn (Continuum)	Combined MOS (0.3–10.0 keV)	Combined MOS (0.6–10.0 keV)	Combined MOS (0.9–10.0 keV)	Combined MOS (1.2–10.0 keV)	Combined MOS (1.5–10.0 keV)
$N(\times 10^{-7})$[a]	143 ± 125	1.6 ± 1.7	1.8 ± 1.9	1.3 ± 1.5	3.2 ± 3.5	1.2 ± 1.5
Γ[a]	1.9 ± 0.1	2.4 ± 0.2	2.4 ± 0.2	2.5 ± 0.2	2.3 ± 0.2	2.4 ± 0.2
C[a]	1.9 ± 0.1	1.9 ± 0.1	1.9 ± 0.1	1.9 ± 0.1	1.9 ± 0.1	1.9 ± 0.1
$N_{\rm QPO}$[b]	... [e]	1.5 ± 0.4	1.5 ± 0.4	1.4 ± 0.4	1.4 ± 0.4	1.0 ± 0.4
ν_0(mHz)[b]	... [e]	6.3 ± 0.2	6.3 ± 0.2	6.2 ± 0.2	6.3 ± 0.2	6.3 ± 0.2
$\Delta\nu$(mHz)[b]	... [e]	1.5 ± 0.5	1.5 ± 0.5	1.7 ± 0.6	1.6 ± 0.6	1.5 ± 0.7
Q[c]	... [e]	4.2	4.2	3.7	3.9	4.2
$\rm rms_{QPO}$[d]	... [e]	11.1 ± 2.5	11.2 ± 2.5	11.9 ± 2.7	12.6 ± 2.9	12.0 ± 3.5
χ^2/dof	354/284	216/189	219/189	215/189	243/189	220/189

Notes.

[a] We fit the continuum with a power-law model described as follows:

$$\text{continuum} = N\nu^{-\Gamma} + C$$

where Γ is the power-law index of the continuum.

[b] We modeled the QPOs with a Lorentzian. The functional form is as follows:

$$\text{QPO} = \frac{N_{\rm QPO}}{1 + \left(\frac{2(\nu - \nu_0)}{\Delta\nu}\right)^2}$$

where ν_0 is the centroid frequency and $\Delta\nu$ is the FWHM of the QPO feature.

[c] The quality factor of the QPO defined as $\nu_0/\Delta\nu$.

[d] The fractional rms amplitude of the QPO (see text).

[e] In this case we only modeled the continuum.

parameters, i.e., a χ^2 of 217 with 189 dof (see the second column of Table 1). This decrease in χ^2 serves as a further indicator of the significance of the QPO component. Using the *F*-test, this corresponds to a single-trial significance of 4×10^{-5}. Note that we essentially searched in a known narrow frequency range of $\approx$5–10 mHz (from the prior *XMM-Newton* observation), and thus the effective number of trials is $\sim$1.

It is clear that the QPO is present in two independent detectors at $>3.5\sigma$ confidence level in each case. The chance probability of two independent 3σ detections alone is 4.33σ. Given the 3.5σ detections in two separate measurements, we conclude that the observed 7 mHz QPO of IC 10 X-1 is statistically highly significant.

In addition, we studied the energy dependence of the fractional rms amplitude of the QPO. For this purpose, we extracted the PDS of the source in seven energy bands. Owing to the low count rate we fixed the upper bound of the bandpass at 10 keV and varied the lower limit from 0.3 to 1.5 keV and constructed

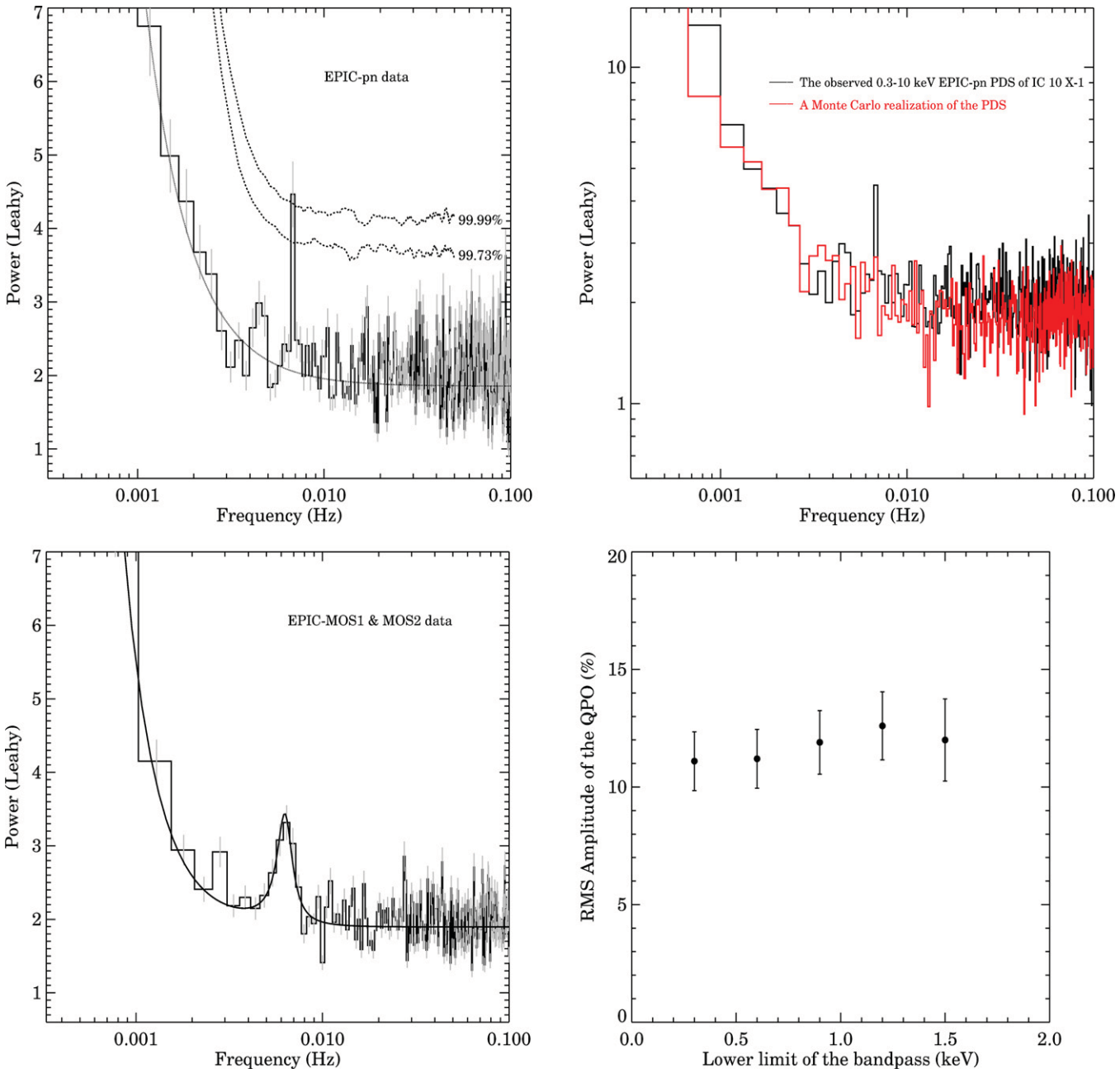

Figure 3. Top left panel: the EPIC-pn PDS of IC 10 X-1 using the longest GTI of 75 ks (black histogram) along with the best-fit power-law model for the continuum (solid). The 99.73% and the 99.99% Monte Carlo simulated confidence contours are also shown (dashed). The QPO at 7 mHz is evident. Top right panel: the observed EPIC-pn PDS of IC 10 X-1 (black: same as the figure on the left) and a sample Monte Carlo simulated PDS (red). Bottom left panel: the combined 0.3–10.0 keV EPIC-MOS PDS of IC 10 X-1 using the longest common GTI of 95 ks (histogram). The best-fit model is also shown (solid). Again the feature at 7 mHz is evident. Bottom right panel: the fractional rms amplitude of the QPO vs. the lower bound of the bandpass used for constructing the PDS. The upper limit was fixed at 10 keV (see text).

a PDS in each case using the combined MOS data. Each of these PDS were then modeled with a power-law plus constant for the continuum and a Lorentzian for the QPO (best-fit model parameters shown in Table 1). The fractional rms amplitude of the QPO is

$$\text{rms amplitude}(\%) = 100\left(\sqrt{\frac{\pi N W}{2C}}\right),$$

where N and W are the normalization and the width of the QPO (Lorentzian), respectively, while C is the mean count rate of the source. The dependence of the rms amplitude of the QPO as a function of the lower limit of the bandpass is shown in the bottom right panel of Figure 3. There is a very weak dependence of the QPO's amplitude on the energy from 0.3 to 1.5 keV. Four of the five PDS used for this analysis are shown in Figure 4. At energies greater than 1.5 keV the low signal-to-noise ratio of the data does not allow us to detect the QPO.

3.1. Search for a Power Spectral Break

Numerous X-ray binaries and also active galactic nuclei show evidence for the presence of a break in their PDS (e.g., McHardy et al. 2006; Markowitz & Edelson 2004). We searched for a spectral break in IC 10 X-1 using the data from the longest GTI

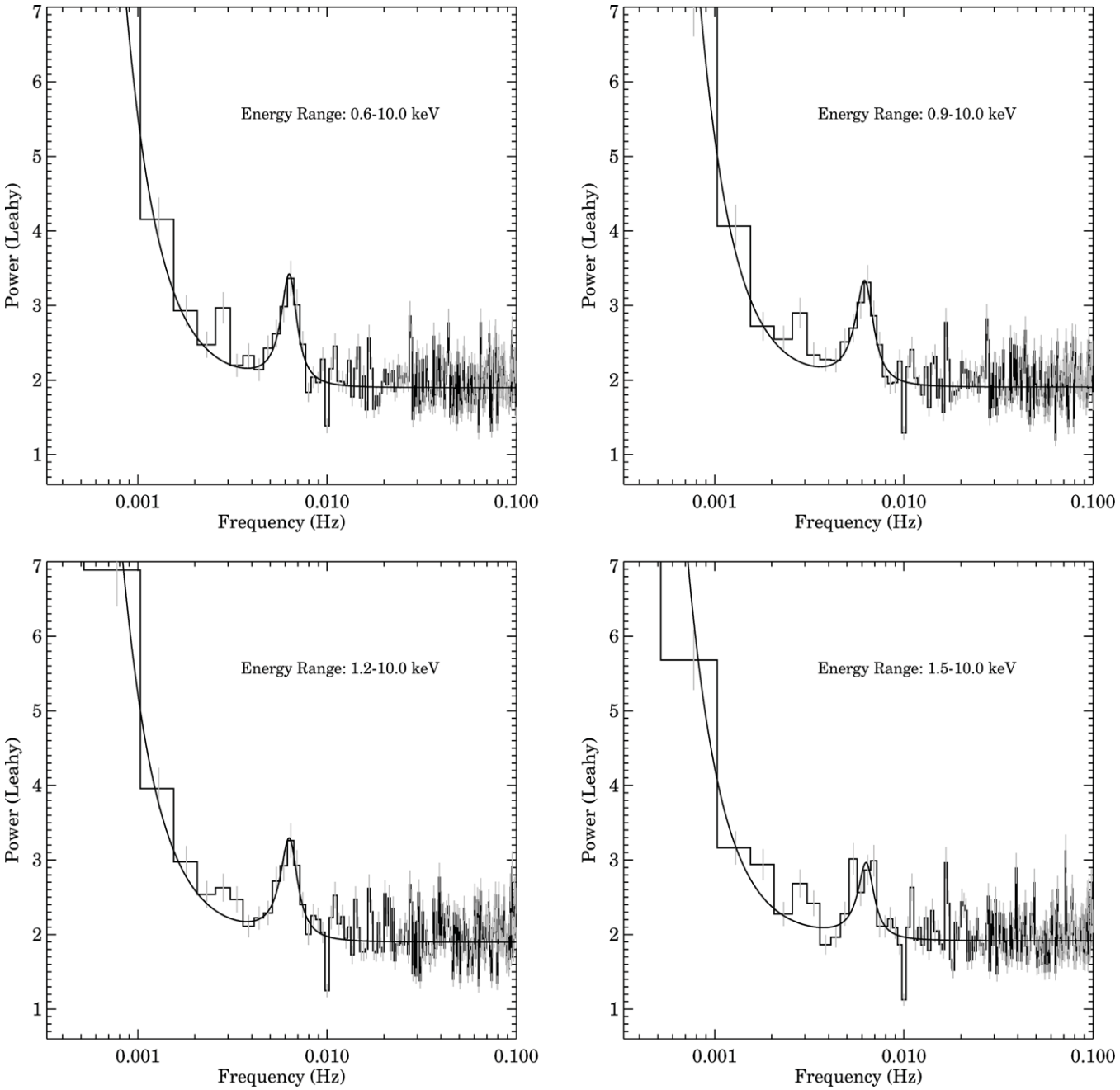

Figure 4. Combined MOS PDS of IC 10 X-1 in various energy bands. The energy band used for the PDS is indicated at the top-right of each panel. The best-fit model (see Table 1) is also overlaid (solid) in each case.

outside the eclipse, i.e., hour 15.5 to 33.5 in Figure 2. Note that the presence of an eclipse in the data adds red noise to the power spectrum that is not intrinsic to the source variability. We constructed the combined MOS 0.3–10.0 keV PDS and did not find any obvious evidence for a PDS break down to frequencies as low as 0.0001 Hz. Note that a single PDS is noisy, with error in a particular bin equal to the value of that bin (van der Klis 1989). Therefore, averaging (say, by combining neighboring bins) is necessary to reduce the noise in the PDS. Hence, even though the lowest sampled frequency is $\approx 10^{-5}$ Hz (1/total length) averaging reduces the lowest effective frequency to roughly 0.0001 Hz in this case. It remains possible that a break may exist at $\lesssim$0.0001 Hz. Moreover, we modeled this PDS with a power-law and a Lorentzian. We find that the best-fit continuum can be described by a power-law of index ≈ -2.

4. DISCUSSION

The frequency of the HFQPOs of StMBHs ($\sim$ a few 100 Hz) and the *hectohertz* QPOs of neutron stars ($\sim$100–300 Hz) are roughly constant in frequency for a given source (van der Klis 2006). They are thought to have a common origin (e.g., Abramowicz et al. 2003) and it has been proposed that the QPO frequency may scale inversely with the mass of the compact object (e.g., see Figure 4.17 of McClintock & Remillard 2006). With a mass of 23–34 $M_{\odot}$ IC 10 X-1's HFQPOs, if any, are expected to occur in the range of a few tens of Hz. Clearly, the 7 mHz QPO of IC 10 X-1 is orders of magnitude slower than this and is very likely not a HFQPO phenomenon.

The typical values of the centroid frequency, rms amplitude and the quality factor (Q = centroid-frequency/QPO-width)

of type-A LFQPOs are ∼8 Hz, $\lesssim$3 and $\lesssim$3, respectively (e.g., Casella et al. 2005). The respective values for type-B LFQPOs are ∼5–6 Hz, ∼2–4 and $\gtrsim$6. Lastly, type-C QPOs occur in a wider range of frequencies—0.1–15 Hz—and have rms amplitudes of 3–20 with Q factors of ∼7–12. The overall nature of the PDS accompanying type-A, B, and C QPOs can be described as weak red noise, weak red noise, and strong flat-topped noise, respectively. Although the continuum of the PDS of IC 10 X-1 is similar to that accompanying type-A or B QPOs, its QPO frequency, rms amplitude and Q value are quite different (compare values in Table 1 with Table 1 of Casella et al. 2005). On the other hand, the centroid frequency of IC 10 X-1's QPO is much lower compared to a typical type-C QPO.

The mHz QPOs (frequency range of ∼10–200 mHz) of ULXs have been argued to be the analogs of the type-C LFQPOs of StMBHs but occurring at a lower frequency (a few tens of mHz compared to the few Hz of StMBHs) due to the presence of intermediate-mass black holes (mass of a few×(100–1000) $M_{\odot}$) within these systems. While the centroid frequency, the rms amplitude and the Q value of the 7 mHz QPO of IC 10 X-1 are comparable to the mHz QPOs of ULXs (e.g., Dheeraj & Strohmayer 2012), there are two aspects that are dissimilar. (1) We do not detect a break in the PDS of IC 10 X-1 whereas breaks have been seen in all the ULXs (e.g., Dewangan et al. 2006). It is known that the break frequency scales with the QPO frequency as $\nu_{\rm break} \sim \nu_{\rm QPO}/9$ (Wijnands & van der Klis 1999). If that were the case for IC 10 X-1, the expected break is at ∼0.7 mHz. It is thus possible that we are unable to detect the break due to our inability to sample variability at very low ($\lesssim$0.7 mHz) frequencies, or the effects of the eclipse. (2) The rms amplitude—at least in the case of the ULX NGC 5408 X-1—is known to increase with energy from 0.3 to 2.0 keV (Strohmayer et al. 2007; Middleton et al. 2011). However, we do not find evidence for such behavior in IC 10 X-1 (see the right panel of Figure 3).

Two black hole sources, GRS 1915+105 and IGR J17091−3624, show mHz QPOs in the so-called "heartbeat" state or the ρ state (e.g., Greiner et al. 1996; Morgan et al. 1997; Belloni et al. 2000; Altamirano et al. 2011). These QPOs are thought to be the result of a radiation pressure instability causing quasi-periodic evaporation followed by refilling of the inner regions of the accretion disk (Lightman & Eardley 1974; Belloni et al. 1997; Neilsen et al. 2011). These mHz QPOs occur at relatively high luminosities (∼10^{38} erg s^{-1}) and at least in GRS 1915+105 appear to be energy-independent in the bandpass from 2 to 30 keV (see Figure 8 of Morgan et al. 1997). Given the similar frequency, comparable rms amplitude (e.g., Altamirano et al. 2011), energy independence (although here energy independence is seen over a different X-ray bandpass) and similar X-ray luminosity[3] (see also Wang et al. 2005) it is possible that the 7 mHz QPO of IC 10 X-1 is related to the "heartbeat" QPOs. Given its low count rate it is, however, not possible to resolve IC 10 X-1's light curve to the same level as GRS 1915+105 or IGR J17091−3624. It will require instruments with larger collecting area to test this hypothesis.

The 7 mHz QPO of IC 10 X-1 is likely not related to the 1 Hz QPOs of AMXPs or the 7–15 mHz QPOs seen in some neutron star systems (e.g., Revnivtsev et al. 2001; Altamirano et al. 2008b). The 1 Hz QPO phenomenon in AMXPs is thought to be due to disk instabilities within the boundary layer of the accretion disk and neutron star magnetosphere (Patruno et al. 2009). Moreover, the 1 Hz QPOs are seen at low luminosities ($<10^{36}$ erg s^{-1}) and can have rms amplitudes as large as 100% (Patruno et al. 2009). Given the high rms amplitude, and that they are likely related to the beginning of the propeller regime, they are probably different from the QPO seen in IC 10 X-1. The 7–15 mHz oscillations in some neutron stars are linked to marginally stable burning of light elements on the surface of the neutron star (e.g., Heger et al. 2007), a process unique to neutron stars.

On the other hand, the 7 mHz QPO may be connected to the 0.6–2.4 Hz "dipper QPOs" of high-inclination neutron stars in the sense that IC 10 X-1 is also highly inclined (see the eclipse in Figure 1 and Silverman & Filippenko 2008). The so-called "dipper QPOs" are only seen from X-ray dipping sources. The dipping is presumably due to obscuration associated with the high inclination (Parmar & White 1988). Their rms amplitudes are ∼10% and are energy-independent in the range of 2–30 keV (see, for example, Figure 4 of Homan et al. 1999). With the present *XMM-Newton* data a similar energy range cannot be probed. However, we note that the QPO's rms amplitude is comparable to those of "dipper QPOs" and appears to be independent of energy in the range from 0.3 to 1.5 keV. More recently, Altamirano & Strohmayer (2012) reported the discovery of an 11 mHz QPO from a black hole candidate H1743-322 (likely highly inclined; Homan et al. 2005) and suggested this could be the first detection of a "dipper QPO" analog in a black hole (candidate) system. The centroid frequency of the "dipper QPOs" is roughly constant over time. If the 7 mHz QPO is indeed a "dipper QPO" then it's centroid frequency should also remain more or less constant. This can be tested with multi-epoch observations of IC 10 X-1 to search for QPO variability.

Finally, we note that the overall PDS and the QPO properties of IC 10 X-1 are also similar to that of Cygnus X-3 (van der Klis & Jansen 1985). They both have the same power-law-like noise at low frequencies—each with roughly the same slope of −2—with a QPO in the mHz regime and barely any power above 0.1 Hz (see the bottom panels of Figure 2 of Koljonen et al. 2011). In addition, the QPOs in both cases have comparable frequencies, rms amplitudes, and coherences (van der Klis & Jansen 1985). The mHz oscillations of Cygnus X-3 are likely associated with major radio flaring events (Koljonen et al. 2011; see, for example, Lozinskaya & Moiseev 2007 and references therein for radio studies of IC 10 X-1). Simultaneous radio and X-ray observations in the future can test whether jet ejection is related to the QPO in IC 10 X-1.

[3] The X-ray (0.3–10.0 keV) energy spectrum of IC 10 X-1 outside the eclipse can be fit with a canonical model consisting of a disk-blackbody and a power-law plus a Gaussian to model the emission feature at ≈0.9 keV. This model gives an acceptable fit with a χ^2 of 165 for 125 degrees of freedom. A detailed spectral analysis is not the subject of this work. Nevertheless, assuming this simple model, the inferred 2–10 keV luminosity at a distance of 0.66 Mpc is ∼10^{38} erg s^{-1}.

REFERENCES

Abramowicz, M. A., Bulik, T., Bursa, M., & Kluźniak, W. 2003, A&A, 404, L21
Altamirano, D., Belloni, T., Linares, M., et al. 2011, ApJL, 742, L17
Altamirano, D., & Strohmayer, T. 2012, ApJL, 754, L23
Altamirano, D., van der Klis, M., Méndez, M., et al. 2008a, ApJ, 687, 488
Altamirano, D., van der Klis, M., Wijnands, R., & Cumming, A. 2008b, ApJL, 673, L35
Barret, D., Boutelier, M., & Miller, M. C. 2008, MNRAS, 384, 1519
Belloni, T. M., & Altamirano, D. 2013, MNRAS, 432, 10
Belloni, T., Klein-Wolt, M., Méndez, M., van der Klis, M., & van Paradijs, J. 2000, A&A, 355, 271
Belloni, T., Mendez, M., King, A. R., van der Klis, M., & van Paradijs, J. 1997, ApJL, 479, L145

Casella, P., Belloni, T., & Stella, L. 2005, ApJ, 629, 403
Dewangan, G. C., Titarchuk, L., & Griffiths, R. E. 2006, ApJL, 637, L21
Dheeraj, P. R., & Strohmayer, T. E. 2012, ApJ, 753, 139
Greiner, J., Morgan, E. H., & Remillard, R. A. 1996, ApJL, 473, L107
Heger, A., Cumming, A., & Woosley, S. E. 2007, ApJ, 665, 1311
Homan, J., Jonker, P. G., Wijnands, R., van der Klis, M., & van Paradijs, J. 1999, ApJL, 516, L91
Homan, J., Miller, J. M., Wijnands, R., et al. 2005, ApJ, 623, 383
Homan, J., Wijnands, R., van der Klis, M., et al. 2001, ApJS, 132, 377
Jonker, P. G., van der Klis, M., Homan, J., et al. 2000, ApJ, 531, 453
Jonker, P. G., van der Klis, M., & Wijnands, R. 1999, ApJL, 511, L41
Koljonen, K. I. I., Hannikainen, D. C., & McCollough, M. L. 2011, MNRAS, 416, L84
Leahy, D. A., Darbro, W., Elsner, R. F., et al. 1983, ApJ, 266, 160
Lightman, A. P., & Eardley, D. M. 1974, ApJL, 187, L1
Lozinskaya, T. A., & Moiseev, A. V. 2007, MNRAS, 381, L26
Markowitz, A., & Edelson, R. 2004, ApJ, 617, 939
McClintock, J. E., & Remillard, R. A. 2006, in Compact Stellar X-ray Sources, ed. W. Lewin & M. van der Klis (Cambridge: Cambridge Univ. Press), 157
McHardy, I. M., Koerding, E., Knigge, C., Uttley, P., & Fender, R. P. 2006, Natur, 444, 730
Méndez, M., van der Klis, M., & Ford, E. C. 2001, ApJ, 561, 1016
Middleton, M. J., Roberts, T. P., Done, C., & Jackson, F. E. 2011, AN, 332, 388
Miller, J. M., Wijnands, R., Homan, J., et al. 2001, ApJ, 563, 928
Morgan, E. H., Remillard, R. A., & Greiner, J. 1997, ApJ, 482, 993
Neilsen, J., Remillard, R. A., & Lee, J. C. 2011, ApJ, 737, 69
Parmar, A. N., & White, N. E. 1988, MmSAI, 59, 147
Pasham, D. R., & Strohmayer, T. E. 2013, ApJ, 771, 101
Patruno, A., Watts, A., Klein Wolt, M., Wijnands, R., & van der Klis, M. 2009, ApJ, 707, 1296
Prestwich, A. H., Kilgard, R., Crowther, P. A., et al. 2007, ApJL, 669, L21
Remillard, R. A., McClintock, J. E., Orosz, J. A., & Levine, A. M. 2006, ApJ, 637, 1002
Remillard, R. A., Sobczak, G. J., Muno, M. P., & McClintock, J. E. 2002, ApJ, 564, 962
Revnivtsev, M., Churazov, E., Gilfanov, M., & Sunyaev, R. 2001, A&A, 372, 138
Silverman, J. M., & Filippenko, A. V. 2008, ApJL, 678, L17
Strohmayer, T. E. 2001, ApJL, 554, L169
Strohmayer, T. E., Mushotzky, R. F., Winter, L., et al. 2007, ApJ, 660, 580
Timmer, J., & Koenig, M. 1995, A&A, 300, 707
van der Klis, M. 1989, in Timing Neutron Stars, ed. H. Ögelman & E. P. J. van den Heuvel (New York: Plenum), 27
van der Klis, M. 2000, ARA&A, 38, 717
van der Klis, M. 2006, in Compact Stellar X-ray Sources, ed. W. Lewin & M. van der Klis (Cambridge: Cambridge Univ. Press), 39
van der Klis, M., & Jansen, F. A. 1985, Natur, 313, 768
van Straaten, S., van der Klis, M., & Méndez, M. 2003, ApJ, 596, 1155
Wang, Q. D., Whitaker, K. E., & Williams, R. 2005, MNRAS, 362, 1065
Wijnands, R. 2004, NuPhS, 132, 496
Wijnands, R., & van der Klis, M. 1999, ApJ, 514, 939